EPJ Web of Conferences **296**, 14009 (2024) https://doi.org/10.1051/epjconf/202429614009
Quark Matter 2023

Particle production in Au+Au collisions at beam energy scan II energies at STAR

Matthew Harasty[1] for the STAR Collaboration

[1]University of California, Davis

Abstract. We report on measurements of light charged hadron production in Au+Au collisions at $\sqrt{s_{NN}}$ = 14.6, 19.6, 27, and 54.4 GeV from the second phase of the beam energy scan (BES-II) program at RHIC. Transverse mass spectra and rapidity density distributions of $\pi^{\pm}$, $K^{\pm}$, p, and $\bar{p}$ are measured as a function of collision energy, centrality, and rapidity. This work extends the previously published BES-I mid-rapidity ($|y| < 0.1$) measurement to a rapidity of 0.9. This new rapidity dependence highlights the effects of baryon stopping for proton yields and the different production mechanisms of $\pi^{\pm}$ and $K^{\pm}$. The relative abundance of these light hadrons indicates different thermodynamic environments at different energies, centralities, and rapidities. The temperature (T) and chemical potentials (μ_B and μ_S) at chemical freeze-out are reported with their dependence on rapidity to further understand the QCD phase diagram.

1 Introduction

Quantum Chromodynamics (QCD), the theory of strong interactions, predicts that at sufficiently high temperature and high energy density, normal nuclear matter converts into a deconfined state of quarks and gluons, known as the Quark-Gluon Plasma (QGP). To investigate the phase diagram of QCD matter, the Relativistic Heavy Ion Collider (RHIC) performed the first phase of the Beam Energy Scan (BES-I) program in 2010.The success of the BES-I program justified the second phase of Beam Energy Scan (BES-II) with higher statistics and detector upgrades. Au+Au collisions at $\sqrt{s_{NN}}$ = 7.7 - 54.4 GeV were collected during 2017-2021, covering a large area of the QCD phase diagram. Through the measurement of light hadron spectra and dN/dy distributions, we are able to extract the temperature and baryon chemical potential as a function of the collision energy, centrality, and rapidity by fitting the yields to thermal models. The spectra and dN/dy are also valuable to theorists to benchmark physics simulations of heavy ion collisions. Sect. 2 explains the methodology of measuring the spectra and dN/dy in STAR. Sect. 3 compares the different production mechanisms of $\pi^{\pm}$, $K^{\pm}$, p, and $\bar{p}$. The rapidity dependence of thermodynamic variables at chemical freeze-out at $\sqrt{s_{NN}}$ = 27 GeV are discussed in Sect. 4. Sect. 5 examines the collective radial flow at kinetic freeze-out at $\sqrt{s_{NN}}$ = 54.4 GeV for mid-rapidity.

2 Particle Identification and Corrections

Two major detectors at STAR are capable of identifying charged hadrons to ultimately measure the rapidity density distributions of pions, kaons and protons. The time projection chamber (TPC) provides the momentum and energy loss (dE/dx) of charged particles. The barrel

time-of-flight (BTOF) detector can measure the precise timing information of particles to help construct a particle mass used for particle identification. The events are partitioned into several centrality classes with the tracks further partitioned into rapidity and $m_T - m_0$ bins. The particle yields are extracted in each bin by fitting the dE/dx and m^2 distributions with Gaussian and Student-T distributions, respectively. These yields are corrected for energy loss through detector materials, tracking efficiency, and acceptance by a study of Monte Carlo simulations of the STAR detector at each energy. The weak decays of hyperons, including Λ, Ξ^-, and Ω^-, contaminate the primordial yields, so the feed-down contributions are estimated by a mixture of UrQMD and mid-rapidity measurements. The primordial $m_T - m_0$ spectra are fitted at low and high p_T to estimate the dN/dy contributions in the regions that we are unable to measure due to acceptance and statistics. The spectra are also fit with alternate functional forms to estimate the systematic uncertainty in the extrapolation. The final dN/dy values are averaged symmetrically across mid-rapidity.

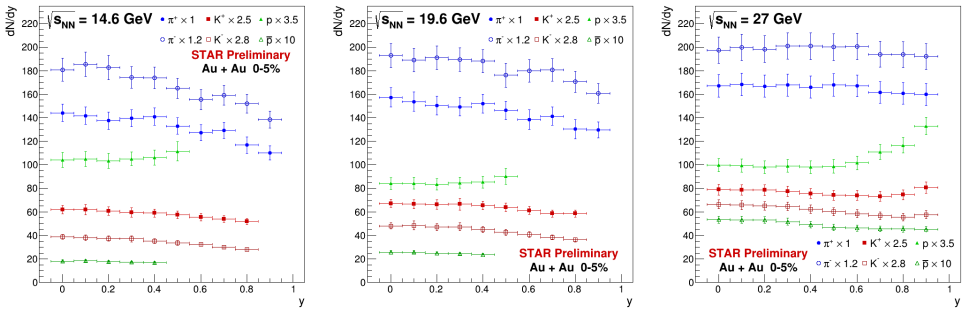

Figure 1. The rapidity density distributions of $\pi^{\pm}$, $K^{\pm}$, p, and $\bar{p}$ in the most central (0-5%) Au+Au collisions at $\sqrt{s_{NN}}$ = 14.6, 19.6, and 27 GeV. The error bars show the combined statistical and systematic uncertainties.

3 dN/dy of Charged Particles

Pair production is the dominant pion production mechanism, but the decays from the Δ resonance and neutron rich initial conditions contribute to an excess of π^- at lower $\sqrt{s_{NN}}$. The dN/dy of pions, kaons, and protons are shown in Fig. 1. Kaons are also produced in pairs, but in less abundance compared to pions due to their mass. An additional channel is available to K^+ through the associated production with a Λ baryon from an interaction of a proton. The uud quarks from proton and an $s\bar{s}$ quark pair form the Λ and K^+. Since there are no anti-protons in the colliding gold nuclei, this channel is suppressed for the K^-, resulting in the differences of the dN/dy distributions of K^+ and K^-. This associated production mechanism contributes less at higher $\sqrt{s_{NN}}$ as pair production dominates. The dN/dy of protons are heavily influenced by the effects of baryon stopping. Baryon stopping quantifies the amount of rapidity loss of the participant nucleons from the initial beam rapidity caused by the interactions with the other colliding nucleus. At mid-rapidity, the shape of the proton dN/dy distribution lowers and widens in more peripheral collisions as well as lower $\sqrt{s_{NN}}$. The change in relative abundances of $\pi^{\pm}$, $K^{\pm}$, p, and $\bar{p}$ in each rapidity region indicates a different thermodynamic environment, discussed in Sect. 4.

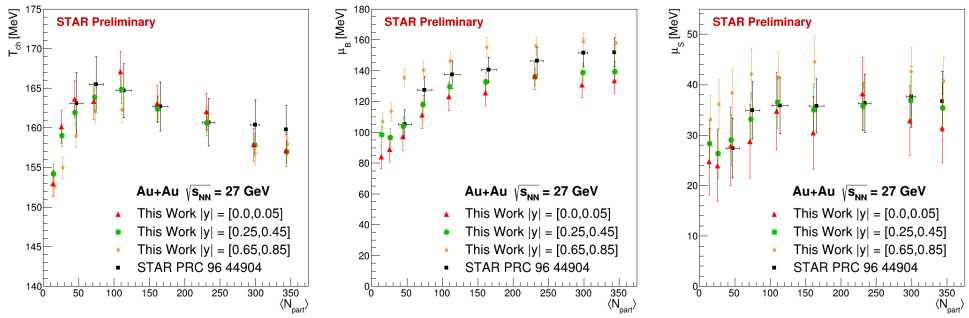

Figure 2. THERMUS calculation of T_{chem} (a), μ_B (b), and μ_S (c) at chemical freeze-out from the yields of $\pi^{\pm}$, $K^{\pm}$, p, and $\bar{p}$ at 27 GeV as a function of $\langle N_{part} \rangle$ in three rapidity bins. The data are compared to the mid-rapidity results of BES-I, which did not include a feed-down correction of protons. Both μ_B and μ_S exhibit a significant rapidity dependence due to baryon stopping and the associated production of K^+.

4 Temperature and Chemical Potential at Chemical Freeze-Out

As the fireball expands, it reaches a stage where the inelastic collisions cease, which is known as chemical freeze-out. At this point, the total yields of each particle species are fixed. Chemical freeze-out is one location we can measure along the matter's trajectory in the QCD phase diagram. This work expands upon the previous mid-rapidity studies of BES-I[1][2] to understand chemical freeze-out as a function of rapidity. Treating each rapidity slice with its own local equilibrium, the dN/dy of the six light hadrons can serve as inputs to THERMUS, a chemical equilibrium model, to extract the temperature, (T_{chem}), baryon chemical potential (μ_B), and strangeness chemical potential (μ_S).

Figure 2 shows the thermodynamic variables at chemical freeze-out at different centralities and rapidities at $\sqrt{s_{NN}} = 27$ GeV. The temperature exhibits a slight centrality dependence, with T_{ch} rising from central to mid-central collisions and falling from mid-central to peripheral collisions. The baryon chemical potential lowers in peripheral collisions due to the fewer nucleon-nucleon collisions for each participating nucleon. The rapidity dependence of μ_B is fairly consistent across different centralities with a $\Delta\mu_B \sim 25$ MeV for a unit change in rapidity. This change in μ_B can be attributed to the differing rapidity distributions for p and $\bar{p}$ from the stopped protons. The previously published BES-I measurement of protons[1][2] did not include a feed-down correction, which explains the discrepancy in μ_B at mid-rapidity in comparison to the new BES-II result. The additional associated production channel for K^+ widens its dN/dy distribution compared to K^-. The third panel of Fig. 2 highlights the rapidity dependence of μ_S with $\Delta\mu_S \sim 10$ MeV for a unit away from mid-rapidity. Despite the net-zero strangeness in the initial conditions, the Λ and K^+ move to different regions of phase space through the process of strangeness distillation[4], resulting in a non-zero strangeness chemical potential.

5 Temperature and Radial Flow Velocity at Kinetic Freeze-Out

After the total yields of particles are fixed at chemical freeze-out, the last elastic collisions occur. This point is known as kinetic freeze-out. These two freeze-out points have been shown to differ when the collision energy rises above $\sqrt{s_{NN}} \approx 7$ GeV[1]. The most central mid-rapidity p_T spectra at $\sqrt{s_{NN}} = 54.4$ GeV are depicted in Fig. 3 are simultaneously fit with

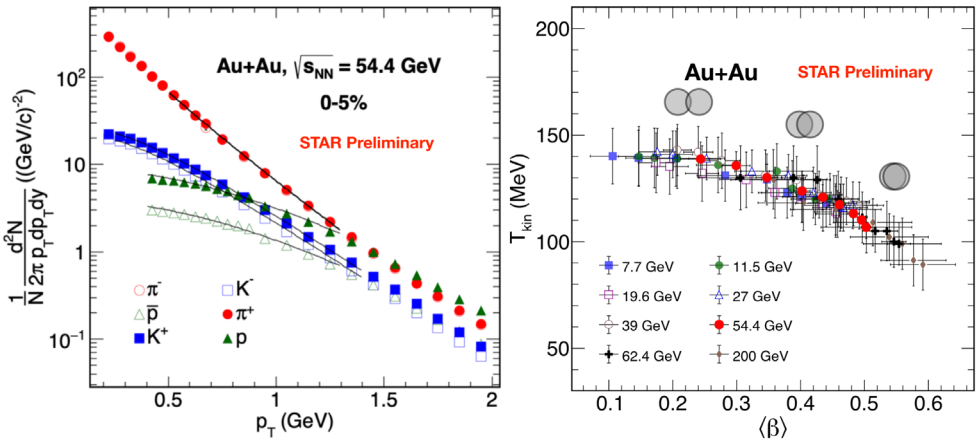

Figure 3. (a) Simultaneous Blast-Wave fit of the mid-rapidity p_T spectra of $\pi^{\pm}$, $K^{\pm}$, p, and $\bar{p}$ at 54.4 GeV. (b) The temperature and the average collective radial flow velocity at kinetic freeze-out for several centrality bins, compared to BES-I measurements.

a Blast-Wave model[3], where all particles share a common temperature (T_{kin}) and average transverse radial flow velocity ($\langle\beta\rangle$) for each centrality bin. Irrespective of collision energy, the T_{kin} and $\langle\beta\rangle$ all lie on the same contour, but the T_{kin} decreases from peripheral to central collisions while $\langle\beta\rangle$ increases. The 54.4 GeV result agrees with the previously established trends at kinetic freeze-out.

6 Summary

The $m_T - m_0$ spectra and dN/dy distributions are presented for $\pi^{\pm}$, $K^{\pm}$, p, and $\bar{p}$ at a subset of BES-II energies at STAR, including $\sqrt{s_{NN}}$ = 14.6, 19.6, 27, and 54.4 GeV. At 54.4 GeV, the collective radial flow velocity and temperature at kinetic freeze-out at mid-rapidity agree well with the other energies of BES-I. These results expand on the previously published BES-I studies at mid-rapidity by examining the rapidity dependence of the rapidity density distributions and thermodynamic variables at chemical freeze-out. The additional production of K^+ in association with a Λ generates a non-zero μ_S that increases with rapidity with $\Delta\mu_S \sim$ 10 MeV for a unit change in rapidity at 27 GeV. The stopped participant protons contribute to the difference in shape of the dN/dy distributions of p and $\bar{p}$, leading to a $\Delta\mu_B \sim 25$ MeV for a unit change in rapidity. These measurements extend our knowledge of the QCD phase diagram by examining how the thermodynamic quantities at chemical freeze-out change with rapidity.

References

[1] STAR Collaboration (L. Adamczyk et al.), Phys. Rev. C **96**, 44904 (2017)
[2] STAR Collaboration (J. Adam et al.), Phys. Rev. C **101**, 24905 (2020)
[3] E. Schnedermann, J. Sollfrank, and U. W. Heinz, Phys. Rev. C **48**, 2462 (1993)
[4] C. Greiner, P. Koch, and H. Stöcker, Phys. Rev. Lett. **58**, 1825 (1987)